Engineering the direct deposition of Si nanoparticles for improved performance in Li-ion batteries

Xu, Yaolin; Borsa, Dana M.; Mulder, Fokko M.

DOI
10.1149/2.0421903jes

Publication date
2019

Document Version
Final published version

Published in
Journal of the Electrochemical Society

JES Focus Issue of Selected Papers from IMLB 2018

Engineering the Direct Deposition of Si Nanoparticles for Improved Performance in Li-Ion Batteries

Yaolin Xu,[1] Dana M. Borsa,[2] and Fokko M. Mulder[1,z]

[1]*Materials for Energy Conversion and Storage (MECS), Department of Chemical Engineering, Faculty of Applied Sciences, Delft University of Technology, 2629 HZ Delft, The Netherlands*
[2]*Meyer Burger (Netherlands) B.V., 5657 EB Eindhoven, The Netherlands*

In our efforts to address the issues of Si based anodes for Li ion batteries, such as limited active mass loading, rapid capacity degradation and low scalability in manufacturing, we reported a scalable, high mass loading, and additive-free Si nanoparticles (NP) deposition based electrode, but the achieved capacity and cycle life were still limited. In order to improve the reversible capacity and cycling stability of this Si NP deposition electrode, in this work, we have investigated various substrates for Si deposition, including carbon paper (CP), preheated CP and stainless steel felt/mesh (SSF/SSM), and their influences on the electrochemical Li-ion storage performance of the Si NP electrodes. Meanwhile, protective encapsulations of amorphous carbon or silicon nitride on Si NP has been performed and the capabilities of these coatings in improving the cycling stability of Si NP electrodes have been researched. It is found that a carbon-coated Si NP deposition on an SSM substrate achieves an extraordinary cycling stability in electrochemical Li-ion storage for 500 cycles with an average capacity loss of 0.09% per cycle, showing significantly improved commercial viability of Si NP deposition based electrodes in high-energy-density Li-ion batteries.

 [DOI: 10.1149/2.0421903jes]

Manuscript submitted October 29, 2018; revised manuscript received December 14, 2018. Published December 28, 2018. *This paper is part of the JES Focus Issue of Selected Papers from IMLB 2018.*

Si based materials have received intensive research attention in the past decade to be used as the anode for Li-ion batteries due to its highest theoretical capacity for Li-ion storage (4200 mAh g^{-1} for $Li_{4.4}Si$).[1–4] However, the uptake of Li ions in Si is unavoidably accompanied with severe volume expansion and irreversible and unstable solid electrolyte interphase (SEI) formation that causes the pulverization of active materials and continuous SEI growth, leading to the loss of active materials, overwhelming electrode structural deformation and thus rapid capacity deterioration and short cycle life.

Immense efforts have been devoted to confining the volume change of Si upon Li-ion storage and stabilizing the electrode during cycling.[5–9] Nanostructuring of Si materials (e.g. nanosphere,[10,11] nanowire,[12,13] nanotube,[14,15] and silicene (2D Si sheet),[16,17] etc.) has achieved extraordinary improvement in its cycling performance by effectively relieving the mechanical strain and accommodating the large volume changes. Moreover, incorporating other components (e.g. carbon,[18–21] polymer,[22–24] metals,[25–27] and oxides,[28–30] etc.) into the nanostructured Si electrodes has also achieved promising electrochemical performance, among which advanced Si-C nanocompositing has been the most successful electrode design in Li-ion batteries. Carbon nanomaterials are present either next to Si as stress buffering matrices to accommodate the strain, or on the surface of Si serving as a mechanically stable and protective layer as well as an artificially engineered SEI to prevent the Si based SEI growth. However, the commercial realization of these nanostructured Si and Si-based composite electrodes is still tremendously challenged by the high cost in advanced binders (e.g. self-healing polymer[31,32] and molecular pulley binder[33]) and conductive additives (e.g. graphene[34–36] and carbon nanotube[37–39]) and/or the complicated production and processing involved in the manufacturing of sophisticated nanostructured Si electrodes.

Si nanoparticles (NP) deposition or thin film has been regarded as one of the most promising solutions to commercialize the Si anodes in Li-ion batteries attributed to multiple advantages:[40] (i) Industrially scalable techniques have been developed for Si deposition, such as chemical vapor deposition (CVD) which has been widely used in solar photovoltaic production with a high throughput and scalability. (ii) It allows the absence of binder, increasing the overall capacity of the electrode. (iii) Si deposition can be performed on any shape with any size,[41,42] demonstrating great potential in a broad scope of application. However, the thickness of Si deposition based electrode is usually rather low (max. 5 μm) and thus the areal mass loading (in [mg cm^{-2}]) and capacity (in [mAh cm^{-2}]) are limited. To address this issue, we have reported a Li-ion battery electrode of a high mass loading (>2 mg cm^{-2}) Si NP deposition on a porous carbon paper (CP) substrate with interconnected nanoscale porosities allowing for the filtration of liquid electrolyte and facilitated Li-ion transport. The Si NP/CP electrode achieved a high capacity (∼ 600 mAh g^{-1} at 0.8 A g^{-1} for 2.0 mg cm^{-2} Si NP) and stable cycling in Li-ion batteries for 100 cycles benefiting from a locally protective SiO_x-derived SEI formation on individual Si NP clusters that maintains the structural stability over cycling.[43] However, the initially irreversible Li loss needs to be reduced, and the cycling stability and cycle life of the Si NP deposition based electrodes still has to be largely improved to enhance the commercial viability.

This article presents a follow-up research on the Si NP deposition based Li-ion battery anode in Ref. 43. In this work, multiple types of substrates, e.g. preheated CP and stainless steel felt/mesh (SSF/SSM), have been used for Si deposition as an alternative for the reference CP. Moreover, surface encapsulation of C or SiN_x on Si NP has been introduced in order to stabilize the electrode and to enhance its cycling stability. The engineered Si NP deposition – Si NP-C/SSM, compared to the previous reported Si NP/CP electrode in Ref. 43, achieves significant improvement in the capacity (>900 mAh g^{-1} at 0.8 A g^{-1} for 2.2 mg cm^{-2} Si NP during the initial cycles) and cycling stability (500 cycles with an average loss of 0.09% per cycle), and showing great promise in its application for the next-generation Li-ion batteries.

Experimental

Electrode fabrication.—The Si deposition was produced via plasma-enhanced chemical vapor deposition (PECVD). To be consistent and comparable with prior results in Ref. 43, the Si deposition has been performed with exactly the same equipment operating at the same conditions as detailed in Ref. 43, and the same denotations (e.g. Si NP deposition/electrode/layer/cluster) have also been used in this article. The deposition was carried out layer by layer with each layer including 30s' deposition of Si NP. Various substrates (12.7 mm in

[z]E-mail: F.M.Mulder@tudelft.nl

diameter, 1.27 cm^2 per electrode), including preheated CP (HTCP, @ 200°C), SSM and SSF, were used for Si NP deposition. Surface coating of C and SiN_x on Si NP was obtained as below:

1. *Si NP-SiN_x/SSM electrodes*: Amorphous SiN_x deposition on Si NP/SSM was carried out with PECVD and the thickness of the SiN_x layer is approximately 500 nm (vs. the Si NP underneath: 10–40 μm).
2. *Si NP-C/SSM electrodes*: C coating on the Si NP was achieved through the pyrolysis of sucrose. Specifically, a Si NP/SSM sample was wetted with a sucrose solution (20 g L^{-1}) and dried in a vacuum oven operating at 70°C. Subsequently the sample was transferred to a tube furnace and, before the pyrolysis, the pyrolysis chamber was purged with argon for 30 min at 100°C to remove the moisture and reactive gases (e.g. O_2) to avoid any (further) oxidation of Si NP and SS during the pyrolysis. Then the temperature was increased stepwise to and kept at 500°C for 60 min to allow the pyrolysis of sucrose; and an argon gas flow ran throughout the process to protect the sample from oxidation and to remove the pyrolyzed product from sucrose. Though the exact amount of C coating on Si NP is still to be determined (as the mass increase per electrode is within the error bar of the balance (±0.05 mg)), it is negligible compared to the mass of Si NP (1.5–3 mg per electrode).

Characterization.—Morphologies of the substrates and the Si NP depositions were imaged with a JEOL JSM 6010F scanning electron microscope (SEM) at 5 kV. High resolution SEM images were obtained with a Hitachi S4800 SEM operating at 15 kV. X-ray photoelectron spectroscopy (XPS) on the Si NP depositions were performed using a Thermo Fisher Scientific X-ray Photoelectron Spectrometer with an Al K_α source; and the spectra were analyzed with a Thermo Avantage software.

Battery assembly and electrochemistry.—The electrochemical performance of the Si NP deposition based electrodes were tested within Li-ion half cells using Li metal as the counter and reference electrode. As-prepared Si NP depositions were used as the working electrodes without further processing. These cells were assembled in an Ar-filled glove-box (H_2O and O_2: <0.1 ppm). A borosilicate glass fibre (Whatman) worked as the separator; and the electrolyte was 1 M lithium hexafluorophosphate ($LiPF_6$) dissolved in ethylene carbonate (EC), diethyl carbonate (DEC) and fluoroethylene carbonate (FEC) (1:1:1 in volume). The electrolyte salt and solvents were purchased from Sigma Aldrich and used as received.

Galvanostatic dis-/charge of the cells were carried out with a MACCOR 4600 battery cycler within a voltage range of 0.01 V and 1.0 V vs. Li^+/Li. In this article, all the reported specific capacities are calculated based on the total mass of Si NP and the C/SiN_x coating (*excl.* the substrate). For the Si NP/HTCP electrodes, the capacity of the CP substrate was determined in Ref. 43 and has been subtracted to obtain the specific capacity of Si NP.

Results and Discussion

Preheating of the CP substrate during si NP deposition.—Figures 1a–1e shows the micro-morphology of a 2-layer Si NP deposition on HTCP, which appears similar to that on the non-heated CP in Ref. 43. What is different is that the thickness of one Si NP layer on HTCP is merely 5 μm, which is approximately a half of that on a normal CP. This is indicative of a twice denser Si NP deposition, resulting from the heated substrate that prevents the major clustering of Si NP upon reaching the substrate leading to a compact deposition. Therefore, it is expected that the surface area of Si NP available for the wetting of liquid electrolyte is largely reduced, and less SEI will be formed.

The electrochemical performance of the Si NP/HTCP electrode has been achieved by galvanostatic dis-/charge of the Si NP/HTCP electrode at 0.8 A g^{-1} in Li-ion half-cells (Figures 1f–1g). The Si NP/HTCP electrode shows an initial reversible capacity of 2918 mAh g^{-1} with a Coulombic efficiency of 77.9%, remarkably better than the reference Si NP/CP electrode that gives an initial capacity of 1222 mAh g^{-1} and a Coulombic efficiency of 49.3%. The high efficiency originates from a low irreversible SEI formation as described above. However, its superiority in electrochemical performance does not last long. Rapid capacity fading happens in the Si NP/HTCP electrode while the reference Si NP/CP electrode remains relatively more stable. The retained reversible capacity of the Si NP/HTCP electrode drops to 1188 mAh g^{-1}, more or less the same as the Si NP/CP electrode, in 50 cycles and keeps close to that of the reference electrode since then. Meanwhile, the Coulombic efficiency of the Si NP/HTCP electrode is higher within the initial 30 cycles and becomes worse after 130 cycles than that of the Si NP/CP electrode. It indicates that, though the reduced surface area causes a limited SEI formation, the more compact deposition is accompanied with a lower inter-particle porosity, which is too limited to sufficiently accommodate the large volume expansion of Si NP upon lithiation. As a result, upon repetitive dis-/charge, significant materials pulverization takes place and the SEI formation is unstable. The beneficial one-off and locally protective SEI formation reported in the reference Si NP/CP electrode does not exist in the Si NP/HTCP electrode.

The voltage profiles of both electrodes (Figures 1h–1i) show typical de-/lithiation voltage responses of Si deposition. It is noted that, in the initial cycles, the dis-/charge overpotentials of the Si NP/HTCP electrode appear lower than that of the Si NP/CP electrode, which is probably due to the lower amount of electronically insulating SEI formation and thus lower internal resistance. As a result, the achieved capacity during the working voltage range is higher. This is also in line with the previous observations.

SS substrates for si NP deposition.—The CP substrate is electrochemically active for lithiation, therefore it deforms over cycling and wears thick electrically insulating SEI films on the carbon fibers (Figure S1), which deteriorates its function as a current collector and compromises the electrochemical performance of the entire electrode. To address this issue, two electrochemical inactive SS substrates, SSM and SSF, have been utilized for Si NP deposition. The morphologies and electrochemical performance of these electrodes were displayed in Figure 2. The SSM substrate shows woven SS wires with a diameter of about 20 μm for individual wires (Figure 2a). In comparison, the wires of SSF are much thinner (~5 μm in diameter, Figures 2b). Similar to the Si NP deposition on carbon fibers of the CP, the Si depositions stay on top of the SS wires consisting nano- and submicro-scale Si NP clusters (Figures 2c–2d and Figure S2). Across the area of the substrates, the Si NP deposition on SSM, compared to that on SSF, is much more uniform thanks to its regular weaving of SS wires, which also allows, next to the inter-particle porosity inside the deposited Si NP clusters, a second larger length scale and structured porosity for the volume expansion during lithiation. Therefore, it is anticipated that, upon lithiation, the Li-ion storage in Si NP/SSM will be homogeneous and the volume expansion of the electrode will be less significant; whereas the presence of the hot spots (relatively more concentrated Si NP areas) on SSF causes more pounced and uneven volume expansion resulting in more noticeable structural deformation over cycling. This is evident in the micrographs of the cycled electrodes (Figures 2e–2f). Thus, the long-term structural stability of Si NP/SSM is significantly higher than Si NP/SSF.

Figure 3 shows the electrochemical properties of the Si NP/SSM and Si NP/SSF electrodes comparing to that of the reference Si NP/CP electrode. The initial reversible capacity for both electrodes reaches above 1500 mAh g^{-1}, noticeably higher than the reference electrode (1222 mAh g^{-1}). Over cycling, the capacity of Si NP/SSF electrode decays rapidly and the retained capacity becomes lower than Si NP/CP after 55 cycles. Though gradual deterioration also takes places in the Si NP/SSM electrode, it is much more stable compared to the Si NP/SSF and Si NP/CP electrodes. The capacity retention in 200 cycles is 896 mAh g^{-1}, corresponding to 58.3% of the initial capacity, which is remarkably higher than Si NP/SSF (32.3%) and Si NP/CP

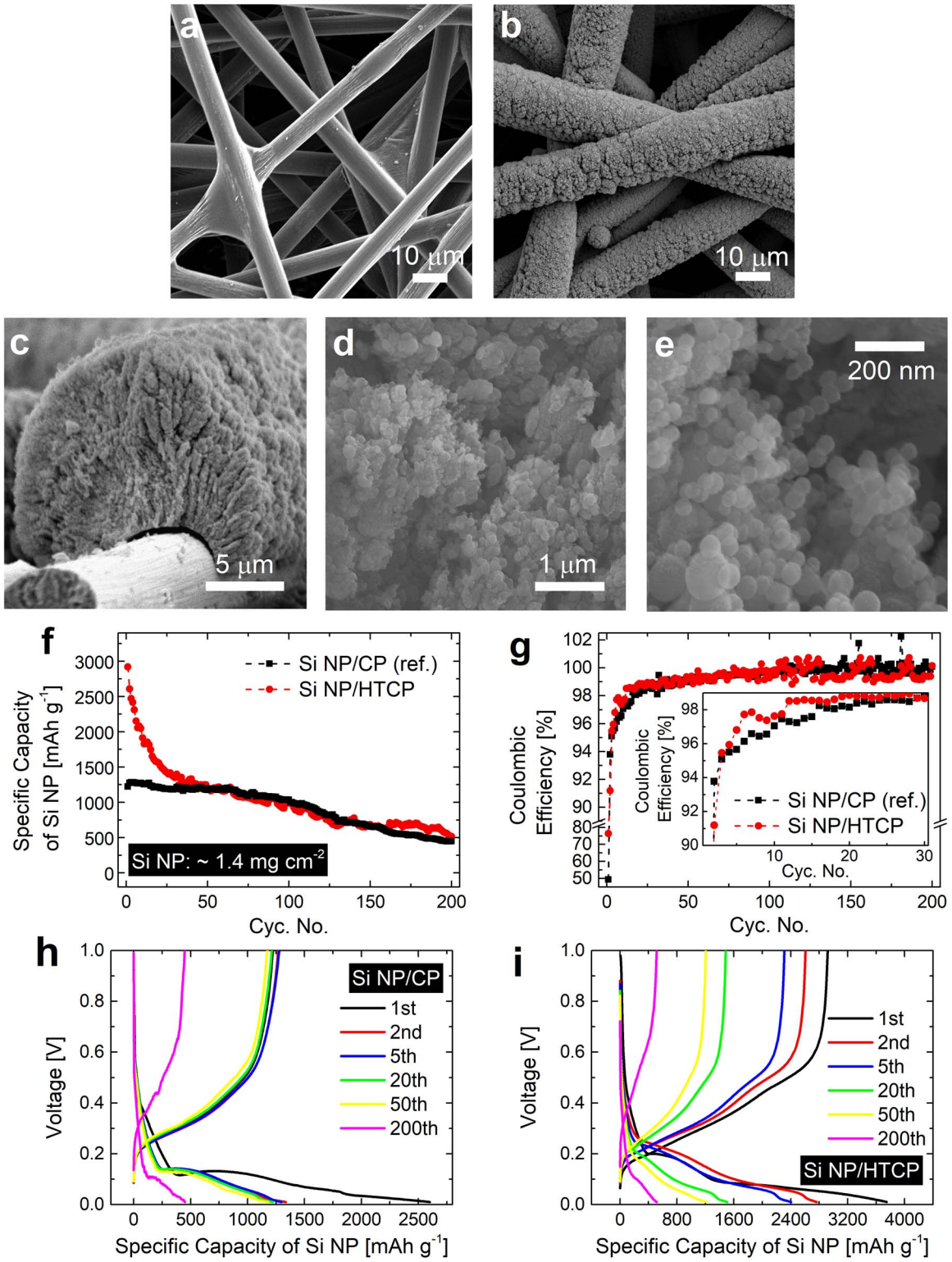

Figure 1. Morphology and electrochemical performance of the Si NP/HTCP electrode. Top-view micrographs of (a) pristine CP and (b) Si NP on HTCP, and (c)–(e) cross-sectional SEM images of the Si NP on HTCP with various magnifications. (f) Specific capacities, (g) Coulombic efficiencies and (h–i) voltage responses of the Si NP/HTCP and reference Si NP/CP electrodes cycling at 0.8 A g^{-1}. Here the mass loading of Si NP is around 1.4 mg cm^{-2}.

(36.7%). The improved capacity of Si NP using SS based current collectors (compared to CP) originates from its higher electronic conductivity and inactivity for lithiation, and hence reduced overpotential and better Coulombic efficiency during dis-/charge. The superior cycling stability of Si NP/SSM than Si NP/SSF results from its lower overpotential and higher Coulombic efficiency during initial cycles, associated with (a) the less profound structural deformation benefiting from the more homogeneous Si deposition and available space for volume expansion as described before, and (b) the low hysteresis in ionic transport thanks to the regular weaving of SSM that facilitates electrolyte channels enabling high ionic conductivity into the electrode.[44]

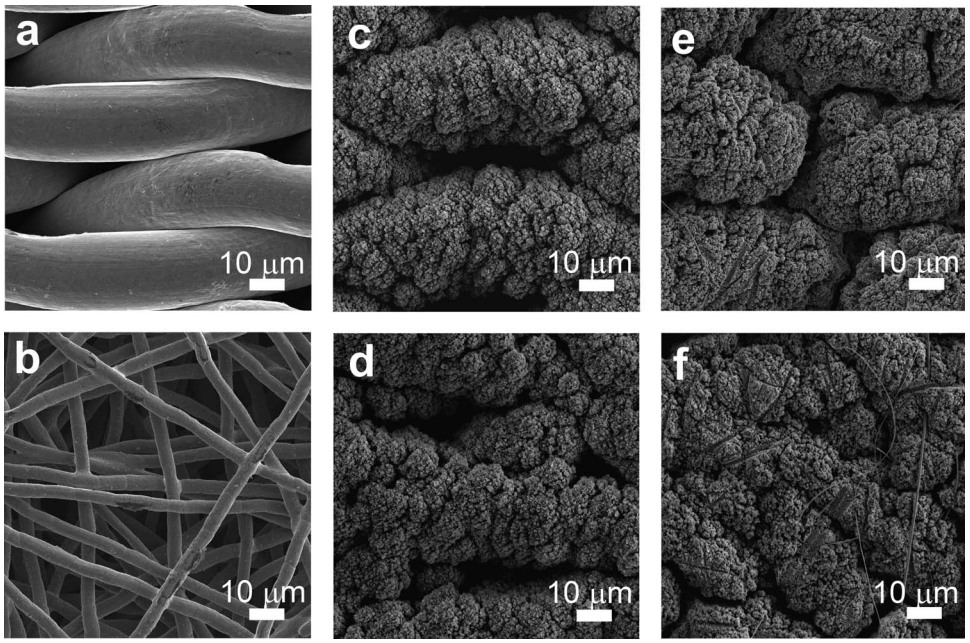

Figure 2. Morphology of the Si NP/SS based electrodes. Micrographs of (a) SSM and (b) SSF substrates, and (c & d) pristine and (e & f) cycled Si NP depositions on SSM and SSF, respectively. Here the cycled electrodes have been dis-/charged at 0.8 A g^{-1} for 200 cycles.

Effects of surface coating (C & SiN_x).—To improve the cycling performance of the Si NP/SSM, surface coating of C or SiN_x has been performed on top of Si NP/SSM to protect and to stabilize the electrode. C coating has been widely used to protect Si electrodes;[45,46] and SiN_x coating has also been reported to be able to improve the electrochemical performance of Si anodes.[47,48]

Figures 4a–4b demonstrate strong peaks of Si-O in both the O 1s and Si 2p spectra, which is indicative of the presence of native oxidation on the surface of Si. The Si peak is also distinct in the Si 2p spectrum, indicating that the native oxide layer is thin (as XPS only detects the surface ∼ few nm). The presence of C coating (as well as organic residual) from the pyrolysis of sucrose on Si NP is extremely thin judging from the high noise ratio of the C 1s spectrum and the presence of Si and Si-O peaks in the Si 2p and O 1s bands (Figures 4c–4e). The SiN_x layer on the (natively oxidized) Si NP is witnessed from the strong Si-N and Si-O-N peaks in the XPS spectra

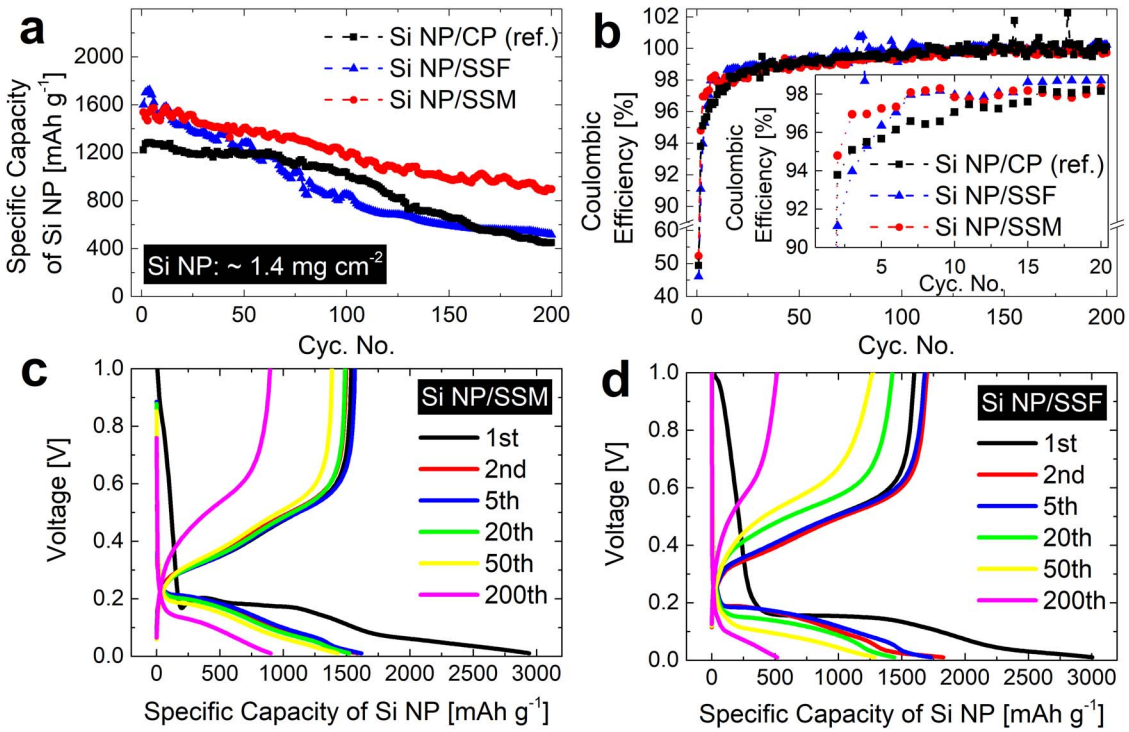

Figure 3. Electrochemical performance of the Si NP/SS based electrodes. (a) Specific capacities, (b) Coulombic efficiencies and (c & d) voltage profiles of Si NP/SS and reference Si/CP electrodes cycling at 0.8 A g^{-1}. Here the mass loading of Si NP is about 1.4 mg cm^{-2}.

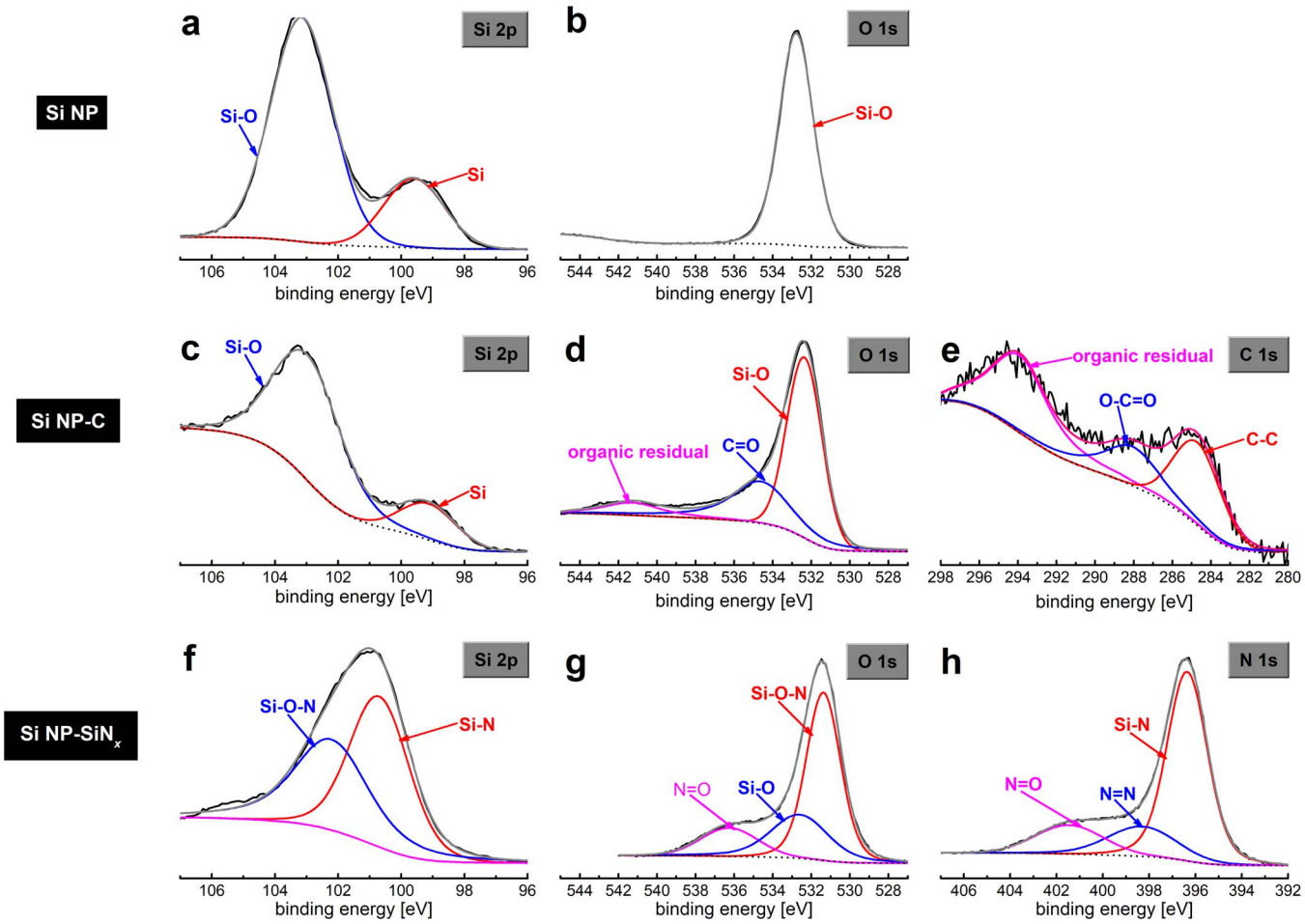

Figure 4. XPS spectra of the Si NP/SSM based electrodes with (a–b) Si NP, (c–e) Si NP-C and (f–h) Si NP-SiN_x on SSM.

obtained on the Si NP-SiN_x sample (Figures 4f–4h), in which the peak from Si is hardly visible due to the high thickness of the SiN_x layer (~500 nm).

Pronounced improvement in the electrochemical performance has been achieved with the surface coating on Si NP deposition. It is observed in Figure 5a that, for Si NP with a high mass loading (2.2 mg cm^{-2}), the Si NP/SSM electrode achieves an initial reversible capacity 1167 mAh g^{-1} for Li-ion storage with a Coulombic efficiency of 49.2%. The retained capacity drops along cycling and amounts to 489 and 195 mAh g^{-1}, 41.9% and 16.7% of the initial value, in 200 and 500 cycles, respectively. The Si NP-SiN_x/SSM electrode exhibits initial improvement in the capacity (1278 mAh g^{-1}) and Coulombic efficiency (59.8%) due to the protection of SiN_x layer. However, rapid fading happens during long-term cycling, and only a capacity of 255 mAh g^{-1} (19.9% of the initial capacity) is retained in 500 cycles. This might be due to the instability and thus continuous growth of SiN_x induced SEI layer and loss of active materials. In comparison, the Si NP/SSM electrode demonstrates remarkable improvement in the cycling stability with C coating. The initial capacity of the Si NP-C/SSM electrode reaches 917 mAh g^{-1}, and the cycling stability of the Si NP electrode is excellent. Specifically, 699 and 495 mAh g^{-1}, 76.2% and 54.1% of the initial capacity, have been achieved in 200 and 500 cycles, respectively. Such a capacity corresponds to an areal Li-ion storage up to 2.0 and 1.1 mAh cm^{-2} for the first and 500th cycle, respectively, with an average loss of 0.09% per cycle.

The enhanced stability in electrochemical cycling is attributed to the improvement in the Coulombic efficiency. It is observed in Figure 5b that the Coulombic efficiencies of the electrodes increase in the order of Si NP/SSM < Si NP-SiN_x/SSM < Si NP-C/SSM, especially in the initial ~150 cycles, revealing that the C-based SEI formation is much more stable than that from SiN_x. The voltage profiles (Figures 5c–5d) of the Si NP-C/SSM and Si NP-SiN_x/SSM electrodes are similar, except that, at the initial stage of the first lithiation of Si NP-SiN_x/SSM, a potential overshoot is present. This is characteristic for a conversion reaction, related to the activation energy required for the nucleation of new phases before the proceeding of the conversion of SiN_x.[49]

Discussions.—This work has researched selective engineering of the substrate and surface coating of Si NP deposition, aimed at improving its electrochemical performance for Li-ion storage.

It demonstrates that preheating of the CP substrate reduces the inter-particle porosity of Si NP deposition, which improves the Coulombic efficiency of the electrode due to the limited SEI formation, but limits its capability of accommodating the volume expansion of Si NP upon Li-ion uptake. As a result, the SEI layer is fractured during cycling and continuous SEI growth occurs, causing the rapid loss of active materials and capacity decay. The replacement of CP substrate with SS avoids the problems associated with the de-/lithiation of CP and promotes the functionality as a current collector. Moreover, the regular weaving of SSM enables homogeneous deposition of Si NP over the substrate area, leading to a high structural stability of Si NP deposition during dis-/charge and hence stable electrochemical cycling. Therefore, the SSM can work as a model system for the engineering of the Si NP deposition substrate to enhance the cycling stability and lifespan of the electrode. However, it should be mentioned that the SSM in this work has limited potential for commercial use as the high thickness and weight of the SSM substrate limits the

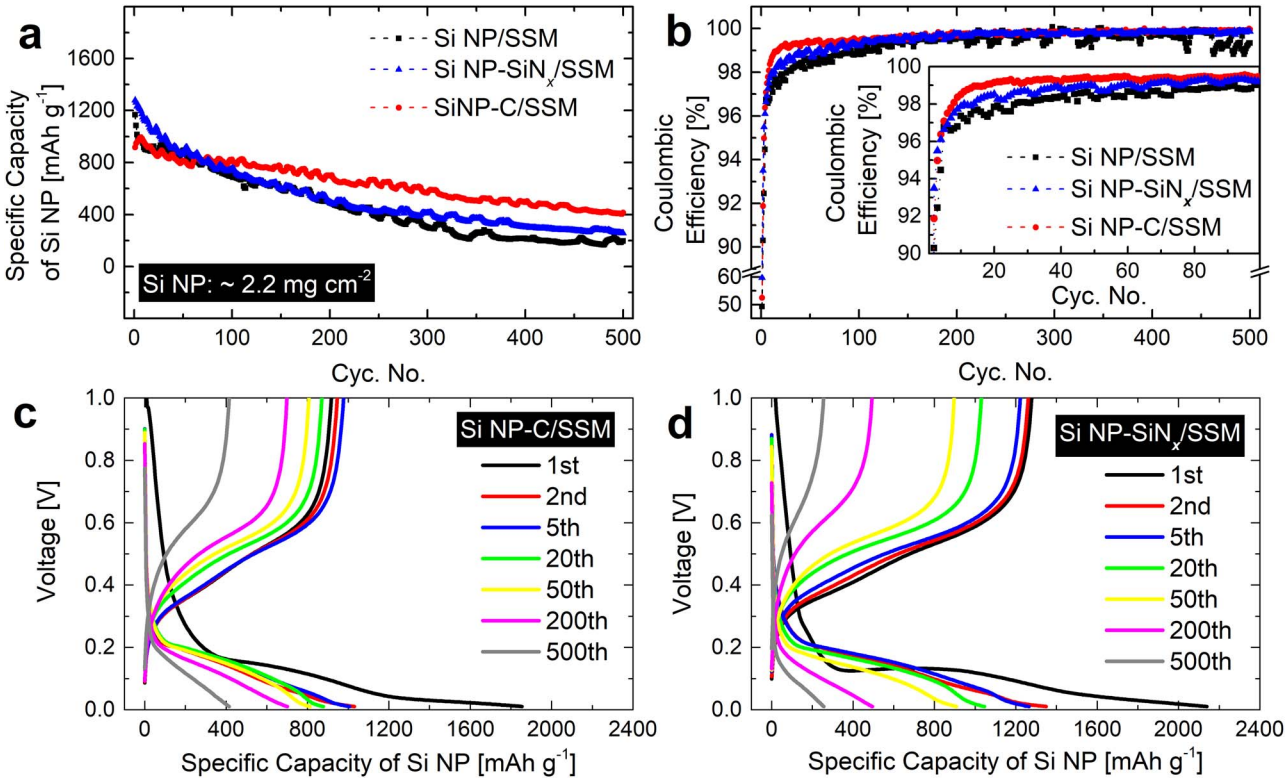

Figure 5. Electrochemical performance of the Si NP/SSM electrodes with SiN_x/C coating. (a) Specific capacities and (b) Coulombic efficiencies and (c & d) voltage curves of these Si NP/SSM based electrodes cycling at 0.8 A g^{-1}. Here the mass loading of Si NP is ~2.2 mg cm^{-2}.

overall capacity of the electrode. The substrate thickness has to be reduced, and the diameter and density of individual SS fibers have to be lowered (e.g. using hollow and thinner wires) concerning its application in practice.

Though the exact form of the conversion reaction of SiN_x remains unclear, it has been proposed that the conversion products can be active Si and inactive Si_3N_4 and/or Li_3N, or Li_xSiN_y ternary phases during the initial lithiation.[50] The Li_3N and Li_xSiN_y exhibit high ionic conductivity facilitating the Li-ion transport, while the inactive Si_3N_4 serves as a structural support for the other phases and a buffer layer to suppress the SEI growth. In this way, it enhances the Coulombic efficiency of de-/lithiation and cycling stability of the Si NP electrode in the initial cycles. However, the positive effects in long-term cycling are rather limited due to the drastic volume changes of Si NP. Moreover, the protection of SiN_x induced SEI layer depends on its thickness. A thinner SiN_x layer (200 nm) results in a more rapid capacity drop (Figure S4c). In comparison, the C-coated Si NP electrode undergoes a more gentle decrease in the capacity retention over cycling, which may possibly be attributed to the improvement in electronic conductivity as well as mitigation of mechanical stress thanks to the presence of C next to Si NP. It works in combination with the locally protective SiO_x-derived SEI layer, maintaining the structural integrity of the electrode. Therefore, the cycling stability and cycle life of the Si NP electrode has been greatly enhanced.

Through the application of SSM current collector and C coating on the Si NP deposition, significant enhancement in the cycling performance has been obtained compared to Ref. 43, in which the reversible capacity of the Si NP/CP electrode (Si NP: 2.0 mg cm^{-2}) amounts to around 600 mAh g^{-1} for 100 cycles. In comparison, the Si NP-C/SSM electrode with a mass loading of 2.2 mg cm^{-2} achieves an initial capacity >900 mAh g^{-1} and stable cycling for 500 cycles.

Considering that Si itself is a semiconductor and the large amount of native SiO_x on the surface of Si as well as its lithiated product (mainly Li_xSiO_y) are electrically insulating, the electrical resistance of the electrode is rather high and notable voltage hysteresis exists during dis-/charge. Therefore, we can expect that the achieved capacity of the Si NP electrode is largely limited by the high overpotential during de-/lithiation, and a lower cycling rate is required to reduce the overpotential and to increase the Li-ion storage capacity within the working voltage range. Figure 6 shows that the capacity undergoes a dramatic rise from 864 mAh g^{-1} to 1517 mAh g^{-1} when the current rate is switched from 0.8 A g^{-1} to 0.2 A g^{-1} at the 201st cycle. However, the capacity drops more rapidly at the lower current rate due to the more drastic volume change and structural deformation during cycling. Therefore, to further upgrade the electrochemical performance of the Si NP deposition electrode, the electrical conductivity of the electrode has to be enhanced for high-rate cycling, and more effective solutions for the confinement of volume changes will be necessary to maintain the structural stability of the electrode during low-rate cycling.

Conclusions

This work presents multiple approaches to enhance the electrochemical performance of Si NP direct deposition based Li-ion battery anodes. It reveals that, compared to a CP substrate (and current collector), a HTCP substrate based Si NP electrode has achieved higher initial reversible capacities but exhibits rapid capacity degradation over cycling; while a SSM substrate has improved the achieved reversible capacity as well as the cycling stability of the Si NP electrode. Moreover, both C and SiN_x coatings on Si NP can improve the Coulombic efficiency (i.e. reversibility) of the electrodes, and the C-coated Si NP electrode exhibits better cycling stability than the SiN_x-coated one.

The combination of a woven SSM current collector and C coating on the Si NP deposition has achieved significant enhancement in the electrochemical performance compared to the previous work. A Si NP-C/SSM electrode with a Si NP loading of 2.2 mg cm^{-2} has obtained a high capacity (917 mAh g^{-1} for the first cycle) and outstanding cycling stability for 500 cycles with a capacity loss of <0.1% per cycle. Taking into account the high Si NP loading that promises

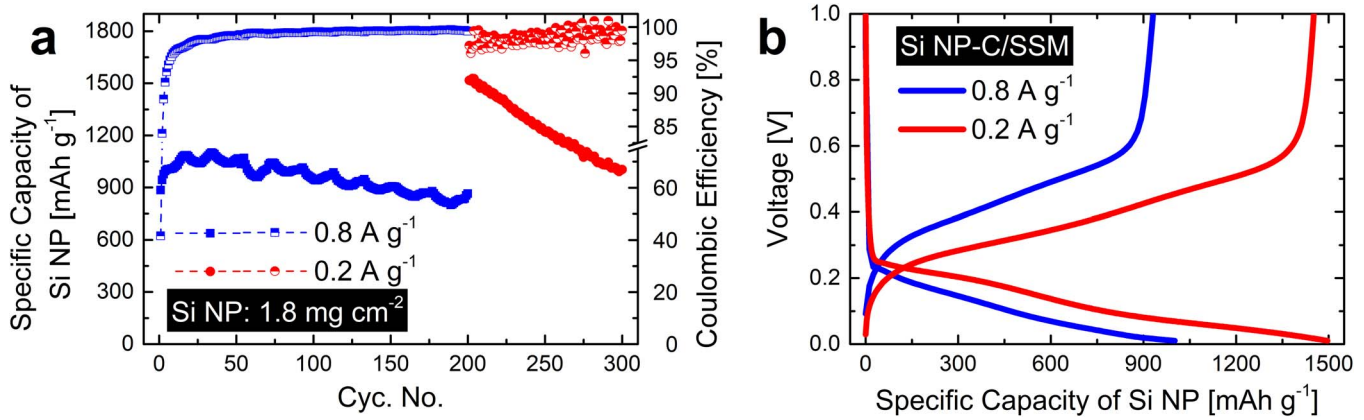

Figure 6. Electrochemical performance of a Si NP-C/SSM electrode. (a) Specific capacities and Coulombic efficiencies cycling at 0.8 A g^{-1} for the first 200 cycles and at 0.2 A g^{-1} during the 200th–300th cycles and (b) voltage profiles of the 5th cycles at 0.8 and 0.2 A g^{-1}, respectively. Here the mass loading of Si NP is ~1.8 mg cm^{-2}.

a high areal Li-ion storage capacity, as well as the high-throughput PECVD based Si NP deposition method enabling scalable electrode manufacturing, this engineered Si NP electrode demonstrates great promise in its commercial introduction in Li-ion batteries.

Acknowledgment

This research is financially supported by A green Deal in innovative Energy Materials (ADEM) grant funded by Dutch Ministry of Economic Affairs and ADEM industrial partners.

ORCID

Yaolin Xu https://orcid.org/0000-0002-2658-3852

References

1. N. Nitta, F. Wu, J. T. Lee, and G. Yushin, *Mater. Today*, **18**, 252 (2015).
2. X. Zuo, J. Zhu, P. Müller-Buschbaum, and Y.-J. Cheng, *Nano Energy*, **31**, 113 (2017).
3. K. Feng, M. Li, W. Liu, A. G. Kashkooli, X. Xiao, M. Cai, and Z. Chen, *Small*, **14**, 1702737 (2018).
4. J.-Y. Li, Q. Xu, G. Li, Y.-X. Yin, L.-J. Wan, and Y.-G. Guo, *Mater. Chem. Front.*, **1**, 1691 (2017).
5. H. Wu and Y. Cui, *Nano Today*, **7**, 414 (2012).
6. X. Su, Q. Wu, J. Li, X. Xiao, A. Lott, W. Lu, B. W. Sheldon, and J. Wu, *Adv. Energy Mater.*, **4**, 1300882 (2014).
7. J. Wang, T. Xu, X. Huang, H. Li, and T. Ma, *RSC Adv.*, **6**, 87778 (2016).
8. A. Franco Gonzalez, N.-H. Yang, and R.-S. Liu, *J. Phys. Chem. C*, **121**, 27775 (2017).
9. H. Kim, E.-J. Lee, and Y.-K. Sun, *Mater. Today*, **17**, 285 (2014).
10. Y. Yao, M. T. McDowell, I. Ryu, H. Wu, N. Liu, L. Hu, W. D. Nix, and Y. Cui, *Nano Lett.*, **11**, 2949 (2011).
11. G. Hou, B. Cheng, Y. Cao, M. Yao, F. Ding, P. Hu, and F. Yuan, *J. Mater. Chem. A*, **3**, 18136 (2015).
12. C. K. Chan, H. Peng, G. Liu, K. McIlwrath, X. F. Zhang, R. A. Huggins, and Y. Cui, *Nat. Nanotechnol.*, **3**, 31 (2008).
13. C. Hwang, K. Lee, H.-D. Um, Y. Lee, K. Seo, and H.-K. Song, *J. Electrochem. Soc.*, **164**, A1564 (2017).
14. H. Wu, G. Chan, J. W. Choi, I. Ryu, Y. Yao, M. T. McDowell, S. W. Lee, A. Jackson, Y. Yang, L. Hu, and Y. Cui, *Nat. Nanotechnol.*, **7**, 310 (2012).
15. Y.-Y. Kim, H.-J. Kim, J.-H. Jeong, J. Lee, J.-H. Choi, J.-Y. Jung, J.-H. Lee, H. Cheng, K.-W. Lee, and D.-G. Choi, *Adv. Eng. Mater.*, **18**, 1349 (2016).
16. J. Zhuang, X. Xu, G. Peleckis, W. Hao, S. X. Dou, and Y. Du, *Adv. Mater.*, **29**, 1606716 (2017).
17. X. Zhang, X. Qiu, D. Kong, L. Zhou, Z. Li, X. Li, and L. Zhi, *ACS Nano*, **11**, 7476 (2017).
18. F. Luo, B. Liu, J. Zheng, G. Chu, K. Zhong, H. Li, X. Huang, and L. Chen, *J. Electrochem. Soc.*, **162**, A2509 (2015).
19. M. Zhang, T. Zhang, Y. Ma, and Y. Chen, *Energy Storage Mater.*, **4**, 1 (2016).
20. Y. Zhang, Y. Zhu, L. Fu, J. Meng, N. Yu, J. Wang, and Y. Wu, *Chin. J. Chem.*, **35**, 21 (2017).
21. X. Shen, Z. Tian, R. Fan, L. Shao, D. Zhang, G. Cao, L. Kou, and Y. Bai, *J. Energy Chem.*, **27**, 1067 (2018).
22. H. Wu, G. Yu, L. Pan, N. Liu, M. T. McDowell, Z. Bao, and Y. Cui, *Nat. Commun.*, **4**, 1943 (2013).
23. M. Kummer, J. P. Badillo, A. Schmitz, H. G. Bremes, M. Winter, C. Schulz, and H. Wiggers, *J. Electrochem. Soc.*, **161**, A40 (2014).
24. Y. Bie, J. Yang, X. Liu, J. Wang, Y. Nuli, and W. Lu, *ACS Appl. Mater. Interfaces*, **8**, 2899 (2016).
25. F. Li, H. Yue, P. Wang, Z. Yang, D. Wang, D. Liu, L. Qiao, and D. He, *CrystEngComm*, **15**, 7298 (2013).
26. W. Ma, X. Liu, X. Wang, Z. Wang, R. Zhang, Z. Yuan, and Y. Ding, *J. Mater. Chem. A*, **4**, 19140 (2016).
27. J. Wu, Z. Zhu, H. Zhang, H. Fu, H. Li, A. Wang, and H. Zhang, *Sci. Rep.*, **6**, 29356 (2016).
28. Y. Bai, D. Yan, C. Yu, L. Cao, C. Wang, J. Zhang, H. Zhu, Y.-S. Hu, S. Dai, J. Lu, and W. Zhang, *J. Power Sources*, **308**, 75 (2016).
29. C. Huang, A. Kim, D. J. Chung, E. Park, N. P. Young, K. Jurkschat, H. Kim, and P. S. Grant, *ACS Appl. Mater. Interfaces*, **10**, 15624 (2018).
30. J. Shin and E. Cho, *Chem. Mater.*, **30**, 3233 (2018).
31. C. Wang, H. Wu, Z. Chen, M. T. McDowell, Y. Cui, and Z. Bao, *Nat. Chem.*, **5**, 1042 (2013).
32. T.-W. Kwon, Y. K. Jeong, I. Lee, T.-S. Kim, J. W. Choi, and A. Coskun, *Adv. Mater.*, **26**, 7979 (2014).
33. S. Choi, T.-W. Kwon, A. Coskun, and J. W. Choi, *Science*, **357**, 279 (2017).
34. Y. Cen, D. R. Sisson, Q. Qin, and J. Liang, *C*, **4**, 18 (2018).
35. E. Greco, G. Nava, R. Fathi, F. Fumagalli, A. E. Del Rio-Castillo, A. Ansaldo, S. Monaco, F. Bonaccorso, V. Pellegrini, and F. Di Fonzo, *J. Mater. Chem. A*, **5**, 19306 (2017).
36. K. Evanoff, A. Magasinski, J. Yang, and G. Yushin, *Adv. Energy Mater.*, **1**, 495 (2011).
37. R. Epur, M. Ramanathan, M. K. Datta, D. H. Hong, P. H. Jampani, B. Gattu, and P. N. Kumta, *Nanoscale*, **7**, 3504 (2015).
38. L. Xue, G. Xu, Y. Li, S. Li, K. Fu, Q. Shi, and X. Zhang, *ACS Appl. Mater. Interfaces*, **5**, 21 (2013).
39. K. Yao, J. P. Zheng, and Z. Liang, *J. Mater. Res.*, **33**, 482 (2018).
40. A. Mukanova, A. Jetybayeva, S.-T. Myung, S.-S. Kim, and Z. Bakenov, *Mater. Today Energy*, **9**, 49 (2018).
41. X. Chen, K. Gerasopoulos, J. Guo, A. Brown, C. Wang, R. Ghodssi, and J. N. Culver, *Adv. Funct. Mater.*, **21**, 380 (2011).
42. A. Mukanova, A. Nurpeissova, A. Urazbayev, S.-S. Kim, M. Myronov, and Z. Bakenov, *Electrochim. Acta*, **258**, 800 (2017).
43. Y. Xu, E. Swaans, S. Chen, S. Basak, P. P. R. M. L. Harks, B. Peng, H. W. Zandbergen, D. M. Borsa, and F. M. Mulder, *Nano Energy*, **38**, 477 (2017).
44. D. P. Singh, F. M. Mulder, A. M. Abdelkader, and M. Wagemaker, *Adv. Eng. Mater.*, **3**, 572 (2013).
45. B. Kim, J. Ahn, Y. Oh, J. Tan, D. Lee, J.-K. Lee, and J. Moon, *J. Mater. Chem. A*, **6**, 3028 (2018).
46. Y. G. Nam, M. Humood, H. Kim, and A. A. Polycarpou, *MRS Commun.*, **7**, 867 (2017).
47. C.-Y. Wu, C.-C. Chang, and J.-G. Duh, *J. Power Sources*, **325**, 64 (2016).
48. S. L. Weeks, N. Leick, and S. Agarwal, *Plasma Processes Polym.*, **13**, 116 (2015).
49. A. Ulvestad, H. F. Andersen, I. J. T. Jensen, T. T. Mongstad, J. P. Mæhlen, Ø. Prytz, and M. Kirkengen, *Sci. Rep.*, **8**, 8634 (2018).
50. A. Ulvestad, J. P. Mæhlen, and M. Kirkengen, *J. Power Sources*, **399**, 414 (2018).